Robotica: (2020) volume 38, pp. 747–759. © Cambridge University Press 2020
doi:10.1017/S0263574719001802

Velocity and Force Transfer Performance Analysis of a Parallel Hip Assistive Mechanism

Jianfeng Li, Leiyu Zhang*, Mingjie Dong, Shiping Zuo, Yandong He and Pengfei Zhang

College of Mechanical Engineering and Applied Electronics Technology, Beijing University of Technology, Beijing, China

(Accepted December 10, 2019. First published online: January 14, 2020)

SUMMARY
Against the backdrop of accelerated ageing around the globe, an increasing number of individuals suffer from hip motion disability and gait disorders. In this paper, the performance analysis of a novel parallel assistive mechanism with 2 DOF for hip adduction/abduction (AB/AD) and flexion/extension (FL/EX) assistance is completed and evaluated, particularly the velocity and force transfer features. The analysis shows that the assistive mechanism has advantages of fine motion assistive isotropy, high force transfer ratio and large force isotropic radius, which indicates that the parallel assistive mechanism is suitable for hip AB/AD and FL/EX assistance.

KEYWORDS: Hip assistance; Parallel mechanism; Performance analysis; Motion assistive isotropy; Force transfer ratio.

1. Introduction

The hip joint plays an important role in human locomotion and weight support. Due to the heavy burden and amount of labor, the motor function of hip joint is easily weakened, and the capacity for walk and other daily activities will be limited.[1–3] Hence, various serial hip exoskeletons have been developed for 1 DOF flexion/extension (FL/EX) assistance. A powered hip exoskeleton[4,5] driven by pneumatic muscles, which was a modified prefabricated orthosis, was presented to assist FL/EX rotation. A light-weight active pelvis orthosis (APO)[6,7] was developed for hip FL/EX assistance, and APO adopted some distinct design aspects: large carbon-fiber parts were used to reduce the inertia, and a novel series elastic actuator unit[8] was designed to increase mechanical compliance. In addition, kinematic compatibility[9,10] and the comfort of physical human–robot interaction (p-HRI)[11] could be improved. A Bowden cable actuation unit was customized for a powered hip exoskeleton (PH-EXOS)[12] to achieve advantages of structure simplicity, light weight and flexible driving. Olivier et al.[13] proposed an assistive motorized hip orthosis (AMPO) for assisting the movements of hip joint in the sagittal plane, and 5 passive DOFs were added to minimize the undesired human–robot interactional loads, thereby improving p-HRI performance. In addition to serial mechanisms, parallel mechanisms consisting of one fixed platform, one mobile platform and several parallel connective branches were also used for hip motion assistance. Compared with serial mechanisms, they have advantages of short power transfer path, high supporting rigidity and large load capacity. Especially, parallel mechanisms are able to keep the revolute center of the mobile platform aligned with the center of hip joint, and hence axis misalignment issues[14,15] in serial hip assistive exoskeletons can be alleviated. Based on the anatomical character analysis of human hip complex, a parallel mechanism[16]

* Corresponding author. E-mail: zhangleiyu@bjut.edu.cn

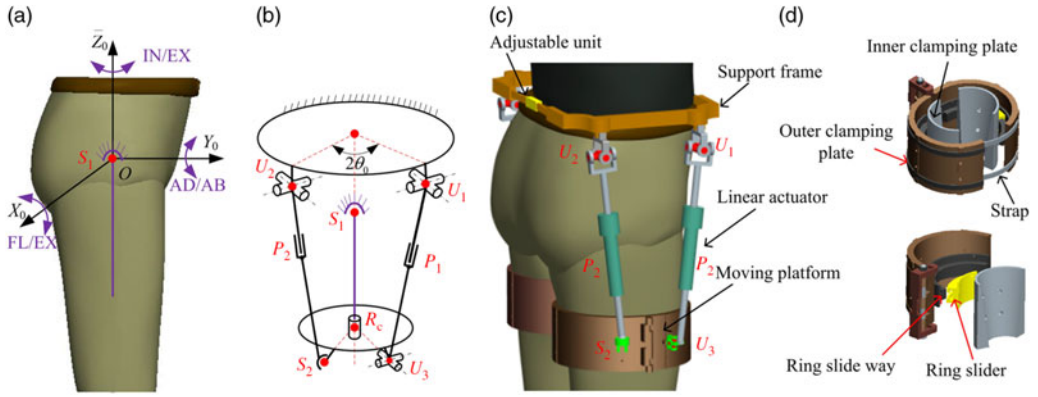

Fig. 1. Parallel assistive mechanism; (a) hip kinematic model; (b) human–machine closed chain; (c) structure of assistive mechanism; (d) detailed structure of joint R_c.

with the 3 PUU configuration was presented to assist hip adduction/abduction (AB/AD), FL/EX and internal/external (IN/EX) rotations, where P and U denote prismatic and universal joints, respectively. Yu et al.[17,18] designed a 3 DOF parallel hip assistive exoskeleton with three UPS parallel branches, where S denotes the spherical joint. In addition, the manipulability inclusive principle was also proposed, and the kinematic parameters of the exoskeleton were optimized to improve its assistive performance. We have presented a novel parallel assistive mechanism with two UPS parallel branches for 2 DOF hip FL/EX and AD/AB assistance,[19] and kinematic interference between the human leg and two branches was analyzed throughout a typical hip assistive gait cycle. The works mentioned above mainly focused on configuration synthesis, kinematic compatibility, light weight and low inertia design, suitable control scheme, prototype development, as well as the performance experimental verification of assistive exoskeletons. Little attention has been placed on performance analysis and capability evaluation of exoskeleton mechanisms, and which is necessary for dimensional parameter optimization, compact structure design and task-space performance improvement of hip assistive exoskeletons.

For the purpose of evaluating the task-space operation capability of industrial robots working with an end-effector, different performance indices, including the dexterity measure, minimum singular value and manipulability ellipsoid, are usually utilized, and these indices can all be defined based on the Jacobian matrices mapping the velocity and force from a robotic joint (actuator) space to the Cartesian (end-effector) space.[20–22] However, unlike end-effector manipulation robots, the task space of a wearable exoskeleton corresponds to the joint space of the human body, and the velocity and force must be transferred from the active joint space of the exoskeleton to the wearer's joint space. Consequently, it is more reasonable to define the evaluation indices on the basis of matrices which reflect the velocity and force mapping relationships between the two joint spaces. In this paper, a parallel assistive mechanism is proposed and described for hip motion disability, gait disorders and healthy people, especially soldiers. Then, its velocity and force transfer performance are mainly analyzed and evaluated. The results presented here are useful for future research on kinematic parameter optimization and structure design of parallel hip assistive mechanism.

2. Kinematic Constraint Equations of the Human–Machine Closed Chain

2.1. Description of parallel assistive mechanism

According to anthropotomy, the human hip complex consists of the femoral head, the cotyle and the ligaments, with the femoral head being able to freely turn in the cotyle. Movements produced at this hip joint are FL/EX, AD/AB and IN/EX rotations, as shown in Fig. 1a. Hence, the hip complex is regarded as a 3-DOF spherical joint denoted by S_1. A coordinate system $O - X_0Y_0Z_0$ is established at the center O of S_1 to depict the three movements clearly. As the motion range and power consumption of the hip IN/EX are much smaller than those of FL/EX and AD/AB movements, a parallel assistive mechanism is proposed for assisting the latter two movements.[19] It is composed of a waist unit, a leg unit and two parallel connective branches (Fig. 1b). The first branch, denoted by $U_1P_1U_3$, consists of a universal joint (U_1), a prismatic joint (P_1) and a universal joint (U_3); the second branch $U_2P_2S_2$

https://doi.org/10.1017/S0263574719001802 Published online by Cambridge University Press

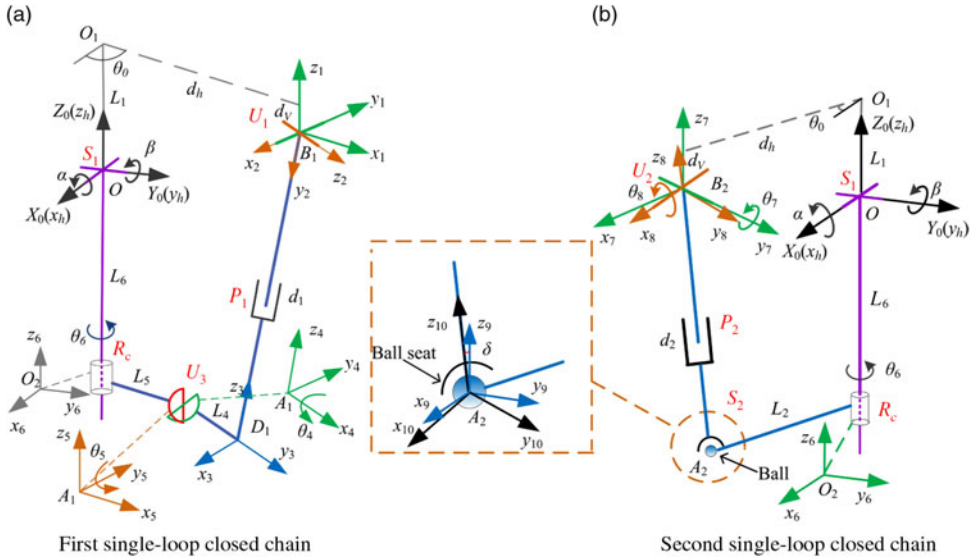

Fig. 2. Establishment of coordinate systems.

includes a universal joint (U_2), a prismatic joint (P_2) and a spherical joint (S_2). The two branches are symmetrically arranged relative to the plane X_0OZ_0, and the initial angle between $U_1P_1U_3$ and $U_2P_2S_2$ is equal to $2\theta_0$. A revolute joint R_c is introduced to adjust IN/EX movement. The hip complex and the thigh are included as part of the human–machine closed chain, and the passive branch S_1R_c is the third branch. Furthermore, a 2-DOF human–machine closed chain can be depicted in Fig. 1b when the assistive mechanism is connected to the hip complex. In this closed kinematic chain, the local DOF around joints S_1 and R_c can be removed as shown in Fig. 2, with the hip joint regarded as a 2-DOF joint with FL/EX and AD/AB mobility.

According to the proposed configuration, a structure was designed as shown in Fig. 1c. A support frame is fixed around the waist and the relevant tautness can be changed by an adjustable unit. The two branches $U_1P_1U_3$ and $U_2P_2S_2$ are installed below the support frame. The other ends are connected to a moving platform. To drive the assistive mechanism, two linear actuators are applied in joints P_1 and P_2, respectively. Joint R_c is mounted inside the moving platform, which is connected to the human thigh, as shown in Fig. 1d. To make it convenient to wear the device, a bearing-like structure is employed in joint R_c. The moving platform consists of two outer clamping plates which are hinged together. The inner clamping plate is worn around the hip thigh. A ring slide way and a ring slider are installed between the outer and inner plates. The inner plate can rotate around the outer one freely. Joint R_c can be bound by woven straps closely.

2.2. *Kinematic constraint equations of the human–machine closed chain*

In the human–machine closed chain (Fig. 1b), the support frame and joint R_c correspond to the fixed and mobile platforms, respectively; their centers are denoted by points O_1 and O_2. In the two parallel branches, the centers of the joints U_3, U_1, S_2 and U_2 are indicated by A_1, B_1, A_2 and B_2, respectively. Then, the parameters of the closed chain can be described as shown in Fig. 2: $OO_1 = L_1$, $O_2A_2 = L_2$, $O_2A_1 = L_5$, $A_1D_1 = L_4$, $OO_2 = L_6$, ${}^hO_1B_i = d_h$ (i.e., the distance between O_1 and B_i in the horizontal direction) and ${}^vO_1B_i = d_v$ (i.e., the distance between O_1 and B_i in the vertical direction). Additionally, for kinetostatic analysis, several reference frames are set up as shown in Fig. 2.

The first single-loop chain consists of branches $U_1P_1U_3$ and S_1R_c, as shown in Fig. 2a. The frames $O - X_0Y_0Z_0$ and $O - x_hy_hz_h$ denote a fixed frame and a movable frame connected with the human thigh, respectively. Their origins are coincident and assigned at the center O of the hip joint. A frame $O_2 - x_6y_6z_6$ is linked with R_c where point O_2 is the center of R_c. The frames $B_1 - x_1y_1z_1$ and $B_1 - x_2y_2z_2$ are assigned at the center B_1 of U_1, where $B_1 - x_1y_1z_1$ denotes a local fixed frame and $B_1 - x_2y_2z_2$ indicates a movable frame connected with the upper link of the first branch $U_1P_1U_3$. The frames $A_1 - x_4y_4z_4$ and $A_1 - x_5y_5z_5$ are assigned at the center A_1 of U_3, connected with the lower link of the first branch and the leg unit, respectively. θ_4 and θ_5 denote the rotation angles of two axes

https://doi.org/10.1017/S0263574719001802 Published online by Cambridge University Press

in the joint U_3. In addition, to facilitate coordinate transformation, a frame $D_1 - x_3y_3z_3$ is set up at point D_1, and the directions of its three coordinate axes are shown in Fig. 2a. In the second single-loop chain (shown in Fig. 2b, and formed by branches $U_2P_2S_2$ and S_1R_c), $B_2 - x_7y_7z_7$ denotes a local fixed frame and $B_2 - x_8y_8z_8$ is a movable frame connected to the branch. Their origins are assigned at the center B_2 of U_2. θ_7 and θ_8 are the rotation angles of two axes in joint U_2. The spherical joint S_2 consists of a ball and a ball seat. The frames $A_2 - x_9y_9z_9$ and $A_2 - x_{10}y_{10}z_{10}$ are connected to the ball and the ball seat, respectively, with their origins at the center A_2 of S_2. δ is the included angle of axes z_9 and z_{10}. When the single-loop closed chain moves, these two frames are maintained parallel to frames $O_2 - x_6y_6z_6$ and $B_2 - x_8y_8z_8$, respectively.

Considering the first single-loop chain, assume it is parted at center A_1. Then, two serial sub-chains $OB_1D_1A_1$ and OO_2A_1 are obtained. According to their kinematic structures, transformation matrices ${}^0\boldsymbol{T}_4$ and ${}^0\boldsymbol{T}_5$, which transfer the coordinates in frames $A_1 - x_4y_4z_4$ and $A_1 - x_5y_5z_5$ to the same frame $O - X_0Y_0Z_0$, respectively, can be written as:

$$ {}^0\boldsymbol{T}_4 = {}^0\boldsymbol{T}_1\,{}^1\boldsymbol{T}_2\,{}^2\boldsymbol{T}_3\,{}^3\boldsymbol{T}_4 = \begin{bmatrix} n_{4x} & n_{4y} & n_{4z} & x_{A1(4)} \\ o_{4x} & o_{4y} & o_{4z} & y_{A1(4)} \\ a_{4x} & a_{4y} & a_{4z} & z_{A1(4)} \\ 0 & 0 & 0 & 1 \end{bmatrix} \tag{1} $$

$$ {}^0\boldsymbol{T}_5 = {}^0\boldsymbol{T}_6\,{}^6\boldsymbol{T}_5 = \begin{bmatrix} n_{5x} & n_{5y} & n_{5z} & x_{A1(5)} \\ o_{5x} & o_{5y} & o_{5z} & y_{A1(5)} \\ a_{5x} & a_{5y} & a_{5z} & z_{A1(5)} \\ 0 & 0 & 0 & 1 \end{bmatrix} \tag{2} $$

where $(n_{ix}, o_{ix}, a_{ix})^T$, $(n_{iy}, o_{iy}, a_{iy})^T$ and $(n_{iz}, o_{iz}, a_{iz})^T$ $(i = 4, 5)$ denote the orientation vectors of axes x_i, y_i, and z_i, respectively. $\boldsymbol{OA}_1 = (x_{A1(4)}, y_{A1(4)}, z_{A1(4)})^T$ and $\boldsymbol{OA}_1 = (x_{A1(5)}, y_{A1(5)}, z_{A1(5)})^T$ indicate the position vectors of center A_1, calculated from sub-chains $OB_1D_1A_1$ and OO_2A_1, respectively. ${}^0\boldsymbol{T}_1$, ${}^1\boldsymbol{T}_2$, ${}^2\boldsymbol{T}_3$, ${}^3\boldsymbol{T}_4$, ${}^0\boldsymbol{T}_6$ and ${}^6\boldsymbol{T}_5$ denote transformation matrices between the two frames, indicated by the subscript and superscript symbols, and given as:

$$ {}^0\boldsymbol{T}_1 = \begin{bmatrix} c\theta_0 & -s\theta_0 & 0 & d_h c\theta_0 \\ s\theta_0 & c\theta_0 & 0 & d_h s\theta_0 \\ 0 & 0 & 1 & L_1 - d_v \\ 0 & 0 & 0 & 1 \end{bmatrix} \quad {}^1\boldsymbol{T}_2 = \begin{bmatrix} -s\theta_1 s\theta_2 & -s\theta_1 c\theta_2 & c\theta_1 & 0 \\ -c\theta_2 & s\theta_2 & 0 & 0 \\ -c\theta_1 s\theta_2 & -c\theta_1 c\theta_2 & -s\theta_1 & 0 \\ 0 & 0 & 0 & 1 \end{bmatrix} $$

$$ {}^2\boldsymbol{T}_3 = \begin{bmatrix} 1 & 0 & 0 & 0 \\ 0 & 0 & -1 & d_1 \\ 0 & 0 & 1 & 0 \\ 0 & 0 & 0 & 1 \end{bmatrix} \quad {}^3\boldsymbol{T}_4 = \begin{bmatrix} 0 & -1 & 0 & 0 \\ 1 & 0 & 0 & -L_4 \\ 0 & 0 & 1 & 0 \\ 0 & 0 & 0 & 1 \end{bmatrix} $$

$$ {}^0\boldsymbol{T}_6 = \begin{bmatrix} c\theta_6 c\beta + s\theta_6 s\alpha s\beta & c\theta_6 s\alpha s\beta - s\theta_6 c\beta & c\alpha s\beta & -L_6 c\alpha s\beta \\ s\theta_6 c\alpha & c\theta_6 c\alpha & -s\alpha & L_6 s\alpha \\ -c\theta_6 s\beta + s\theta_6 s\alpha c\beta & s\theta_6 s\beta + c\theta_6 s\alpha c\beta & c\alpha s\beta & -L_6 c\alpha c\beta \\ 0 & 0 & 0 & 1 \end{bmatrix} \quad {}^6\boldsymbol{T}_5 = \begin{bmatrix} c\theta_0 & -s\theta_0 & 0 & L_5 c\theta_0 \\ s\theta_0 & c\theta_0 & 0 & L_5 s\theta_0 \\ 0 & 0 & 1 & 0 \\ 0 & 0 & 0 & 1 \end{bmatrix} $$

in which c and s are abbreviations of cos and sin, θ_1 and θ_2 indicate the two rotation angles of U_1 (around axes R_{11} and R_{12}, respectively), d_1 denotes the displacement of joint P_1, α and β stand for FL/EX and AD/AB angles of the hip joint around axes x_h and y_h, respectively, and θ_6 is the rotation angle of R_c.

According to the geometrical characteristic of universal joint U_3, the coordinates of center A_1 calculated from sub-chains $OB_1D_1A_1$ and OO_2A_1 are equal and the two revolute axes of U_3

https://doi.org/10.1017/S0263574719001802 Published online by Cambridge University Press

are orthogonal. Hence, the kinematic constraint equations of the first single-loop chain can be expressed as:

$$\begin{cases} x_{A1(4)} = x_{A1(5)} \\ y_{A1(4)} = y_{A1(5)} \\ z_{A1(4)} = z_{A1(5)} \\ n_{4y}n_{5z} + o_{4y}o_{5z} + a_{4y}a_{5z} = 0 \end{cases} \tag{3}$$

where $x_{A1(4)} = a_1c\theta_1 + a_2d_1s\theta_1c\theta_2 + a_3d_1s\theta_2 + a_4$, $y_{A1(4)} = b_1c\theta_1 + b_2d_1s\theta_1c\theta_2 + b_3d_1s\theta_2 + b_4$, $z_{A1(4)} = d_1s\theta_1 + d_2 - d_1c\theta_1c\theta_2$, $x_{A1(5)} = e_1s(\theta_6 + \theta_0) + e_2c(\theta_6 + \theta_0) + e_3$, $y_{A1(5)} = f_1s(\theta_6 + \theta_0) + f_2$, $z_{A1(5)} = g_1c(\theta_6 + \theta_0) + g_2s(\theta_6 + \theta_0) + g_3$, $n_{4y} = -s\theta_0c\theta_2 + s\theta_2c\theta_0s\theta_1$, $o_{4y} = c\theta_0c\theta_2 + s\theta_2s\theta_0s\theta_1$, $a_{4y} = s\theta_2c\theta_1$, $n_{5z} = c\alpha s\beta$, $o_{5z} = -s\alpha$, $a_{5z} = c\alpha c\beta$.
in which

$a_1 = -L_4c\theta_0$, $a_2 = -c\theta_0$, $a_3 = -s\theta_0$, $a_4 = d_hc\theta_0$, $b_1 = -L_4s\theta_0$, $b_2 = -s\theta_0$, $b_3 = c\theta_0$, $b_4 = d_hs\theta_0$, $e_1 = L_5s\alpha c\beta$, $e_2 = L_5c\beta$, $e_3 = -L_6c\alpha s\beta$, $d_1 = L_4$, $d_2 = L_1 - d_v$, $f_1 = L_5c\alpha$, $f_2 = L_6s\alpha$, $g_1 = -L_5s\beta$, $g_2 = L_5s\alpha c\beta$, $g_3 = -L_6c\alpha c\beta$.

According to the kinematic structure of the second single-loop chain, the position vector of center A_2 of spherical joint S_2 determined from the sub-chains OB_2A_{12} and OO_2A_2 should be equal. Hence, the following kinematic constraint equations are obtained:

$$\begin{cases} \boldsymbol{OA}_2 = \boldsymbol{OO}_2 + {}^0\boldsymbol{R}_6\boldsymbol{O}_2\boldsymbol{A}_2 \\ \boldsymbol{OA}_2 = d_2\boldsymbol{z}_8 + \boldsymbol{OB}_2 \end{cases} \tag{4}$$

where d_2 denotes the displacement of joint P_2, $\boldsymbol{OO}_2$ and $\boldsymbol{OB}_2$ denote the position vectors of centers O_2 and B_2, $\boldsymbol{O}_2\boldsymbol{A}_2$ denotes the position vector of center A_2 described in frame $O_2 - x_6y_6z_6$, ${}^0\boldsymbol{R}_6$ indicates the orientation matrix of frame $O_2 - x_6y_6z_6$ relative to frame $O - X_0Y_0Z_0$. The above parameters are given as:

$$\boldsymbol{OO}_2 = (-L_6c\alpha s\beta \quad L_6s\alpha \quad -L_6c\alpha c\beta)^{\mathrm{T}}$$

$$\boldsymbol{O}_2\boldsymbol{A}_2 = (L_2c\theta_0 \quad -L_2s\theta_0 \quad 0)^{\mathrm{T}}$$

$$\boldsymbol{OB}_2 = (d_hc\theta_0 \quad -d_hs\theta_0 \quad L_1 - d_v)^T$$

$${}^0\boldsymbol{R}_6 = \boldsymbol{R}(y_h, \beta)\boldsymbol{R}(x_h, \alpha)\boldsymbol{R}(z_h, \theta_6) = \begin{bmatrix} c\theta_6c\beta + s\theta_6s\alpha s\beta & c\theta_6s\alpha s\beta - c\beta s\theta_6 & c\alpha s\beta \\ c\alpha s\theta_6 & c\theta_6c\alpha & -s\alpha \\ c\beta s\theta_6s\alpha - c\alpha s\beta & s\theta_6s\beta + c\theta_6c\beta s\alpha & c\alpha c\beta \end{bmatrix}$$

3. Jacobian Matrices and Performance Evaluation Indices

In this section, the velocity and force Jacobian matrices of the parallel hip assistive mechanism are derived, and three performance indices, that is, motion assistive isotropy, force transfer ratio and force isotropic radius, are proposed for the task-space performance evaluation of the assistive mechanism.

3.1. Velocity and force Jacobian matrices

Differentiating the kinematic constraint Eq. (3) of the first single-loop chain, we obtain:

$$\begin{cases} H_1\dot{\theta}_1 + H_2\dot{\theta}_2 + H_3\dot{\beta} + H_4\dot{\alpha} + H_5\dot{\theta}_6 + H_6\dot{d}_1 = 0 \\ I_1\dot{\theta}_1 + I_2\dot{\theta}_2 + I_3\dot{\beta} + I_4\dot{\alpha} + I_5\dot{\theta}_6 + I_6\dot{d}_1 = 0 \\ K_1\dot{\theta}_1 + K_2\dot{\theta}_2 + K_3\dot{\beta} + K_4\dot{\alpha} + K_5\dot{\theta}_6 + K_6\dot{d}_1 = 0 \\ Q_1\dot{\theta}_1 + Q_2\dot{\theta}_2 + Q_3\dot{\beta} + Q_4\dot{\alpha} + Q_5\dot{\theta}_6 = 0 \end{cases} \tag{5}$$

where $\dot{\theta}_1$, $\dot{\theta}_2$ and $\dot{\theta}_6$ denote the angle velocities of joints R_{a1}, R_{a2} and R_c, respectively; $\dot{\alpha}$ and $\dot{\beta}$ indicate the angle velocities of hip AD/AB and FL/EX rotations; $\dot{d}_1$ denotes the linear velocity of joint P_1.

https://doi.org/10.1017/S0263574719001802 Published online by Cambridge University Press

The coefficients H_i, I_i, K_i $(i = 1, 2 \ldots 6)$ and Q_i $(i = 1, 2 \ldots 5)$ are:

$$H_1 = -d_1 s\theta_0 c\theta_1 c\theta_2 + L_4 c\theta_0 s\theta_1, H_2 = -d_1 s\theta_0 c\theta_2 + d_1 c\theta_0 s\theta_1 s\theta_2, H_3 = L_5 s\beta c(\theta_6 + \theta_0) + L_6 c\alpha c\beta - L_5 s\alpha c\beta s(\theta_6 + \theta_0),$$
$$H_4 = -L_5 c\alpha s\beta s(\theta_6 + \theta_0) - L_6 s\alpha s\beta, H_5 = L_5 c\beta s(\theta_6 + \theta_0) - L_5 s\alpha s\beta c(\theta_6 + \theta_0),$$
$$H_6 = -c\theta_0 s\theta_1 c\theta_2 - s\theta_0 s\theta_2,$$
$$I_1 = -d_1 s\theta_0 c\theta_1 c\theta_2 + L_4 s\theta_0 s\theta_1, I_2 = d_1 c\theta_0 c\theta_2 + S_1 s\theta_0 s\theta_1 s\theta_2, I_3 = 0, I_4 = L_5 s\alpha s(\theta_6 + \theta_0) - L_6 c\alpha,$$
$$I_5 = -L_5 c\alpha c(\theta_6 + \theta_0), I_6 = -s\theta_0 s\theta_1 c\theta_2 + c\theta_0 s\theta_2,$$
$$K_1 = L_4 c\theta_1 + d_1 s\theta_1 c\theta_2, K_2 = d_1 c\theta_1 s\theta_2, K_3 = L_5 c\beta c(\theta_6 + \theta_0) + L_5 s\alpha s\beta s(\theta_6 + \theta_0) - L_6 c\alpha s\beta,$$
$$K_4 = -L_5 c\alpha c\beta s(\theta_6 + \theta_0) - L_6 s\alpha c\beta, K_5 = -L_5 s\beta s(\theta_6 + \theta_0) - L_5 s\alpha c\beta c(\theta_6 + \theta_0), K_6 = -c\theta_1 c\theta_2,$$
$$Q_1 = c\theta_0 c\theta_1 s\theta_2 c\alpha s\beta - s\theta_0 c\theta_1 s\theta_2 s\alpha - s\theta_1 s\theta_2 c\alpha c\beta, Q_3 = -s\theta_0 c\theta_2 c\alpha c\beta + c\theta_0 s\theta_1 s\theta_2 c\alpha c\beta - c\theta_1 s\theta_2 c\alpha s\beta,$$
$$Q_2 = s\theta_0 s\theta_2 c\alpha s\beta + c\theta_0 s\theta_1 c\theta_2 c\alpha s\beta + c\theta_0 s\theta_2 s\alpha - s\theta_0 s\theta_1 c\theta_2 s\alpha + c\theta_1 c\theta_2 c\alpha c\beta, Q_4 = s\theta_0 c\theta_2 s\alpha s\beta - c\theta_0 s\theta_1 s\theta_2 s\alpha s\beta - c\theta_0 c\theta_2 c\alpha - s\theta_0 s\theta_1 s\theta_2 c\alpha - c\theta_1 s\theta_2 s\alpha c\beta, Q_5 = 0.$$

Then, mapping relationships between $(\dot{d}_1 \quad \dot{\theta}_6)^T$ and $(\dot{\alpha} \quad \dot{\beta})^T$ can be expressed as:

$$\begin{bmatrix} \dot{d}_1 \\ \dot{\theta}_6 \end{bmatrix} = \begin{bmatrix} M_{11} & M_{12} \\ M_{21} & M_{22} \end{bmatrix}^{-1} \begin{bmatrix} N_{11} & N_{12} \\ N_{21} & N_{22} \end{bmatrix} \begin{bmatrix} \dot{\alpha} \\ \dot{\beta} \end{bmatrix} = \begin{bmatrix} J_{11} & J_{12} \\ J_{21} & J_{22} \end{bmatrix} \begin{bmatrix} \dot{\alpha} \\ \dot{\beta} \end{bmatrix} \tag{6}$$

where

$$M_{11} = Q_1^2(H_6 I_2 - H_2 I_6) + Q_1 Q_2(H_1 I_6 - H_6 I_1)$$
$$M_{12} = Q_1^2(H_5 I_2 - H_2 I_5) + Q_1 Q_2(H_1 I_5 - H_5 I_1) + Q_1 Q_5(H_2 I_1 - H_1 I_2)$$
$$M_{21} = Q_1^2(H_6 K_2 - H_2 K_6) + Q_1 Q_2(H_1 K_6 - H_6 K_1)$$
$$M_{22} = Q_1^2(H_5 K_2 - H_2 K_5) + Q_1 Q_2(H_1 K_5 - H_5 K_1) + Q_1 Q_5(H_2 K_1 - H_1 K_2)$$
$$N_{11} = Q_1^2(H_2 I_4 - H_4 I_2) + Q_1 Q_2(H_4 I_1 - H_1 I_4) + Q_1 Q_4(H_1 I_2 - H_2 I_1)$$
$$N_{12} = Q_1^2(H_2 I_3 - H_3 I_2) + Q_1 Q_2(H_3 I_1 - H_1 I_3) + Q_1 Q_3(H_1 I_2 - H_2 I_1)$$
$$N_{21} = Q_1^2(H_2 K_4 - H_4 K_2) + Q_1 Q_2(H_4 K_1 - H_1 K_4) + Q_1 Q_4(H_1 K_2 - H_2 K_1)$$
$$N_{22} = Q_1^2(H_2 K_3 - H_3 K_2) + Q_1 Q_2(H_3 K_1 - H_1 K_3) + Q_1 Q_3(H_1 K_2 - H_2 K_1)$$
$$J_{11} = \frac{M_{22}N_{11} - M_{12}N_{21}}{M_{11}M_{22} - M_{12}M_{21}} \quad J_{12} = \frac{M_{22}N_{12} - M_{12}N_{22}}{M_{11}M_{22} - M_{12}M_{21}} \quad J_{21} = \frac{M_{11}N_{21} - M_{21}N_{11}}{M_{11}M_{22} - M_{12}M_{21}}$$
$$J_{22} = \frac{M_{11}N_{22} - M_{21}N_{12}}{M_{11}M_{22} - M_{12}M_{21}}$$

Differentiating the first equation of Eq. (4), velocity vector $\boldsymbol{V}_{A,2}$ of center A_2 of S_2 can be obtained as:

$$\boldsymbol{V}_{A,2} = \boldsymbol{V}_{O,2} + \boldsymbol{\omega} \times ({}^{O}\boldsymbol{R}_6 \boldsymbol{O}_2 \boldsymbol{A}_2) = \begin{bmatrix} v_{11} & v_{12} \\ v_{21} & v_{22} \\ v_{31} & v_{32} \end{bmatrix} \begin{bmatrix} \dot{\alpha} \\ \dot{\beta} \end{bmatrix} \tag{7}$$

https://doi.org/10.1017/S0263574719001802 Published online by Cambridge University Press

where $\boldsymbol{V}_{O,2}$ denotes the velocity of center O_2, $\boldsymbol{\omega}$ denotes the angle velocity of link O_2A_2, and $v_{ij}(i = 1, 2, 3, j = 1, 2)$ are given as:

$$\begin{aligned}
v_{11} &= L_6 s\alpha s\beta \\
v_{12} &= -L_6 c\alpha c\beta + L_2 c\theta_0 (c\beta s\alpha s\theta_6 - c\alpha s\beta) - L_2 s\theta_0 (s\theta_6 s\beta + c\theta_6 c\beta s\alpha) \\
v_{21} &= L_6 c\alpha - (L_2 c\theta_0 (c\beta c\alpha c\theta_6 - c\alpha c\beta) - L_2 s\theta_0 (s\theta_6 s\beta + c\theta_6 c\beta s\alpha)) \\
v_{22} &= 0 \\
v_{31} &= L_6 s\alpha c\beta + L_2 c\theta_0 s\theta_6 c\alpha - L_2 s\theta_0 c\theta_6 c\alpha \\
v_{32} &= L_6 c\alpha s\beta - (L_2 c\theta_0 (c\theta_6 c\beta + s\theta_6 s\alpha s\beta) + L_2 s\theta_0 (c\beta s\theta_6 - c\theta_6 s\alpha s\beta))
\end{aligned}$$

Differentiating the second equation of Eq. (4) and projecting the velocity vector $\boldsymbol{V}_{A,2}$ of center A_2 on $\boldsymbol{z}_8$ axis, the following expression can be obtained:

$$\dot{d}_2 = V_{z,8} = \boldsymbol{z}_8^T \boldsymbol{V}_{A,2} \tag{8}$$

where $V_{z,8}$ denotes the velocity component of $\boldsymbol{V}_{A,2}$ in z_8 axis direction, $\boldsymbol{z}_8$ is the direction vector of z_8 axis and $\dot{d}_2$ indicates the linear velocity of P_2.

According to Eqs. (7) and (8), $\dot{d}_2$ can be rewritten as:

$$\dot{d}_2 = \begin{bmatrix} J_{31} & J_{32} \end{bmatrix} \begin{bmatrix} \dot{\alpha} \\ \dot{\beta} \end{bmatrix} \tag{9}$$

where $J_{31} = v_{31}$ and $J_{32} = v_{32}$.

Amalgamating the first row of Eq. (6) with Eq. (9), the velocity mapping relationship between the active joint space of the assistive mechanism and human hip joint space can be expressed as:

$$\begin{bmatrix} \dot{\alpha} \\ \dot{\beta} \end{bmatrix} = \boldsymbol{J}_v \dot{\boldsymbol{d}} = \begin{bmatrix} \dfrac{J_{32}}{J_{11}J_{32} - J_{12}J_{31}} & \dfrac{-J_{12}}{J_{11}J_{32} - J_{12}J_{31}} \\ \dfrac{-J_{31}}{J_{11}J_{32} - J_{12}J_{31}} & \dfrac{J_{11}}{J_{11}J_{32} - J_{12}J_{31}} \end{bmatrix} \begin{bmatrix} \dot{d}_1 \\ \dot{d}_2 \end{bmatrix} \tag{10}$$

where $\boldsymbol{J}_v$ denotes the velocity Jacobian matrix of the parallel hip assistive mechanism.

Furthermore, by applying the virtual work principle, the force mapping relationship between the two joint spaces can be written as:

$$\begin{bmatrix} \tau_\alpha \\ \tau_\beta \end{bmatrix} = \boldsymbol{J}_f \begin{bmatrix} f_1 \\ f_2 \end{bmatrix} = \boldsymbol{J}_v^T \begin{bmatrix} f_1 \\ f_2 \end{bmatrix}. \tag{11}$$

where f_1 and f_2 denote the driving forces of joints P_1 and P_2, τ_α and τ_β denote the torques acting on hip AD/AB and FL/EX revolute axes, and $\boldsymbol{J}_f$ denotes the force Jacobian matrix of the assistive mechanism.

3.2. Velocity and force transfer performance indices

3.2.1. Motion assistive isotropy. Using the manipulability ellipsoid definition proposed by Yoshikawa,[20] velocity super-circularity $\dot{\boldsymbol{d}}^T \dot{\boldsymbol{d}} = 1$ is set up in the actuator space of the assistive mechanism. Then this super-circularity can be mapped by the velocity Jacobian matrix $\boldsymbol{J}_v$ into the hip joint space, defined in the fame $O_{h-x_h y_h z_h}$ connected with human thigh, as the following velocity ellipse:

$$\dot{\boldsymbol{d}}^T \dot{\boldsymbol{d}} = \dot{\boldsymbol{\theta}}_h^T \left(\boldsymbol{J}_v \boldsymbol{J}_v^T\right)^{-1} \dot{\boldsymbol{\theta}}_h = 1 \tag{12}$$

where $\dot{\boldsymbol{d}} = (\dot{d}_1 \quad \dot{d}_2)^T$ and $\dot{\boldsymbol{\theta}}_h = (\dot{\alpha} \quad \dot{\beta})^T$.

According to the physical meaning of the velocity ellipsoid, it is known that at a certain movement configuration of the human–machine closed chain, the hip joint obtains the greatest (or least) motion dexterity along the long (or short) principal axis direction of the velocity ellipse. If the velocity ellipse approximates to a circumference, the hip joint gets almost the same motion dexterity along all

https://doi.org/10.1017/S0263574719001802 Published online by Cambridge University Press

directions. Such a movement configuration can be referred to as isotropic configuration. To describe and evaluate assistive isotropy, an index d_a is defined as:

$$d_a = l_{vsp}/l_{vlp} \tag{13}$$

where l_{vlp} and l_{vsp} correspond to the lengths of the long and short principal axes of the velocity ellipse, respectively.

3.2.2. Force transfer ratio. As sufficient torque is critical for hip joint assistance, the force transfer ratio is another important performance indicator in addition to motion assistive isotropy. Similar to velocity ellipse, a force ellipse can be defined as:

$$\boldsymbol{f}^T\boldsymbol{f} = \tau^T \left(\boldsymbol{J}_f\boldsymbol{J}_f^T\right)^{-1} \tau = 1 \tag{14}$$

where $f = (f_1 \quad f_2)^T$ and $\tau = (\tau_\alpha \quad \tau_\beta)^T$.

According to literature,[23,24] it is known that at a certain movement configuration of an end-effector manipulation robot, the force transfer ratio along a particular operation direction is equal to the distance from the center to the surface of force manipulability ellipsoid along the directional vector. Thereby, the robot gets the greatest (or least) force transfer ratio along the long (or short) principle directions of the force ellipsoid. Moreover, a larger least force transfer ratio indicates that the robot is at a movement configuration with a higher force transfer capability. Length l_{fsp} of the short principle axis can be used as an evolution index of force transfer performance. Similarly, force transfer index e_a of this assistive mechanism can be defined as:

$$e_a = l_{fsp} \tag{15}$$

3.2.3. Isotropic force radius. While the manipulability ellipsoid-based indices are popular and have been widely used to evaluate the operation performance of end-effector manipulation robots, they are all independent of the real physical capability of robots' joint actuators (i.e., velocity and force limits of joint actuators are not considered) and hence unable to describe the robot's performance sufficiently. To overcome this defect, alternative indices, including isotropic velocity radius, isotropic acceleration radius and isotropic force radius, were proposed in the literature,[25–27] which were defined and calculated on the basis of task-space capability sets (or polytopes) of manipulation robots.[28,29] As force limits of joint actuators are taken into account, the evaluation index of the isotropic force radius is introduced into the task-space force performance analysis of assistive mechanism.

Let $f_{1\max}$ and $f_{2\max}$ denote the maximum driving forces of linear actuators in branches $U_1P_1U_3$ and $U_2P_2S_2$, respectively. Then, the set $\boldsymbol{T}_f$ of allowable actuator forces can be defined as:

$$T_f = \{\boldsymbol{f} | \quad |f_i| \le f_{i\max} \quad i = 1, 2\} \tag{16}$$

Eq. (16) corresponds to a convex parallelogram with four vertices and four straight edges. As mapped by Eq. (11), a task-space force set $\boldsymbol{T}_t$ is generated in human hip joint space and can be defined as:

$$T_\tau = \left\{ \tau | \quad \tau = \boldsymbol{J}_f\boldsymbol{f} \quad \boldsymbol{f} \in T_f \right\} \tag{17}$$

Since the mapping of Eq. (11) is linear and the joint force set $\boldsymbol{T}_f$ is convex, the task-space force set $\boldsymbol{T}_\tau$ is also convex. Its vertices and edges are the images of vertices and edges of set $\boldsymbol{T}_f$, respectively. The mapping relationship between the two force sets can be generally described by Fig. 3.

According to the above analysis and force mapping relationship shown in Fig. 3, it can be seen that at any movement configuration of the human–machine closed chain, the parallel hip assistive mechanism corresponds to a certain task-space force set $\boldsymbol{T}_t$ determined by the force Jacobian matrix $\boldsymbol{J}_f$. Moreover, there is a certain inscribed circle in the task-space force set $\boldsymbol{T}_\tau$, and radius $r_{i\tau}$ of the inscribed circle indicates the largest assistive torque which can be realized by the assistive mechanism in all directions of human hip joint space, when force limits of the two linear joint actuators are taken into account. Hence, radius $r_{i\tau}$ of the inscribed circle can be adopted as an index for force isotropic evaluation and described as:

$$r_{it} = \text{the value of inscribed circle radius of the task} - \text{space force sets } T_t \tag{18}$$

https://doi.org/10.1017/S0263574719001802 Published online by Cambridge University Press

Table I. Parameters of the human–machine closed chain.

Parameter	d_v/mm	L_1/mm	L_2/mm	d_h/mm	L_4/mm	L_5/mm	L_6/mm	l/(°)
Value	40	80	120	160	20	100	355	60

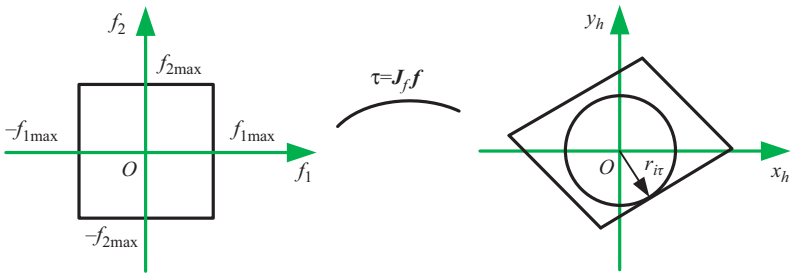

Fig. 3. Mapping relationship between two force sets T_f and T_t.

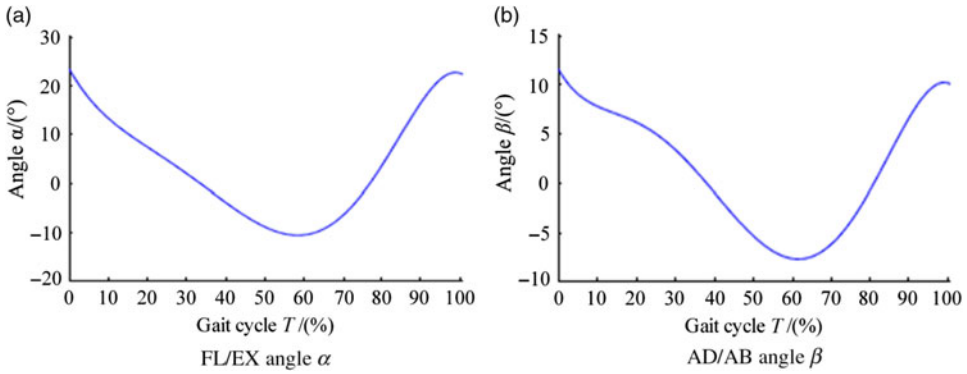

Fig. 4. Hip joint trajectories during a human gait cycle T.

4. Velocity and Force Transfer Performance Analyses of Assistive Mechanism

In this section, motion assistive isotropy d_a, force transfer ratio e_a and isotropic force radius $r_{i\tau}$ of the parallel hip assistive mechanism are calculated during a typical gait assistive cycle. Furthermore, velocity and force transfer performances of the assistive mechanism are evaluated. Without loss of generality, here the force limits of linear actuators in the two branches are assumed as $f_{1\,\max} = f_{2\,\max} = 1$. Dimensional parameters of the human–machine closed chain were determined according to the body parameter measurements of a healthy volunteer (age = 26, height = 175.5 cm and weight = 68.5 kg) and are presented in Table I. Hip AD/AB and FL/EX angle trajectories during a typical human gait cycle denoted by T are shown in Fig. 4, and they were obtained using a VICON motion capturing system.

Applying the position solution proposed in literature[19] and adopting the trajectories of FL/EX and AD/AB angles, shown in Fig. 4, as motion inputs of the human–machine closed chain, both active and passive joint displacements in the assistive mechanism during a human gait cycle are calculated, as shown in Fig. 5. The kinematics of assistive mechanism can be comprehended thoroughly; especially the results of displacements d_1 and d_2 are very helpful to the dynamic stability control system of assistive mechanism for tracking the human walking gait.

Using the analysis and evaluation indices proposed in Section 3, velocity and force transfer performances of the parallel assistive mechanism are investigated. The three performance indices during a typical gait cycle T are calculated, and their trajectories are given in Figs. 6a and 7. Additionally, velocity ellipses, task-space force sets $\boldsymbol{T}_\tau$ and their inscribed circles at 0%, 20%, 40%, 60% and 80% T are shown in Figs. 6 and 8, respectively. L-axis and S-axis are the abbreviations of long and short axes in Fig. 6.

https://doi.org/10.1017/S0263574719001802 Published online by Cambridge University Press

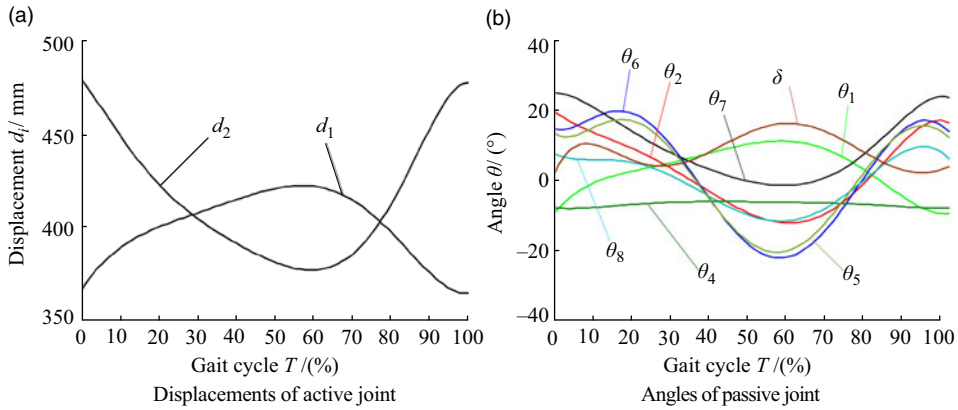

Fig. 5. Kinematics of the parallel assistive mechanism during a human gait cycle T.

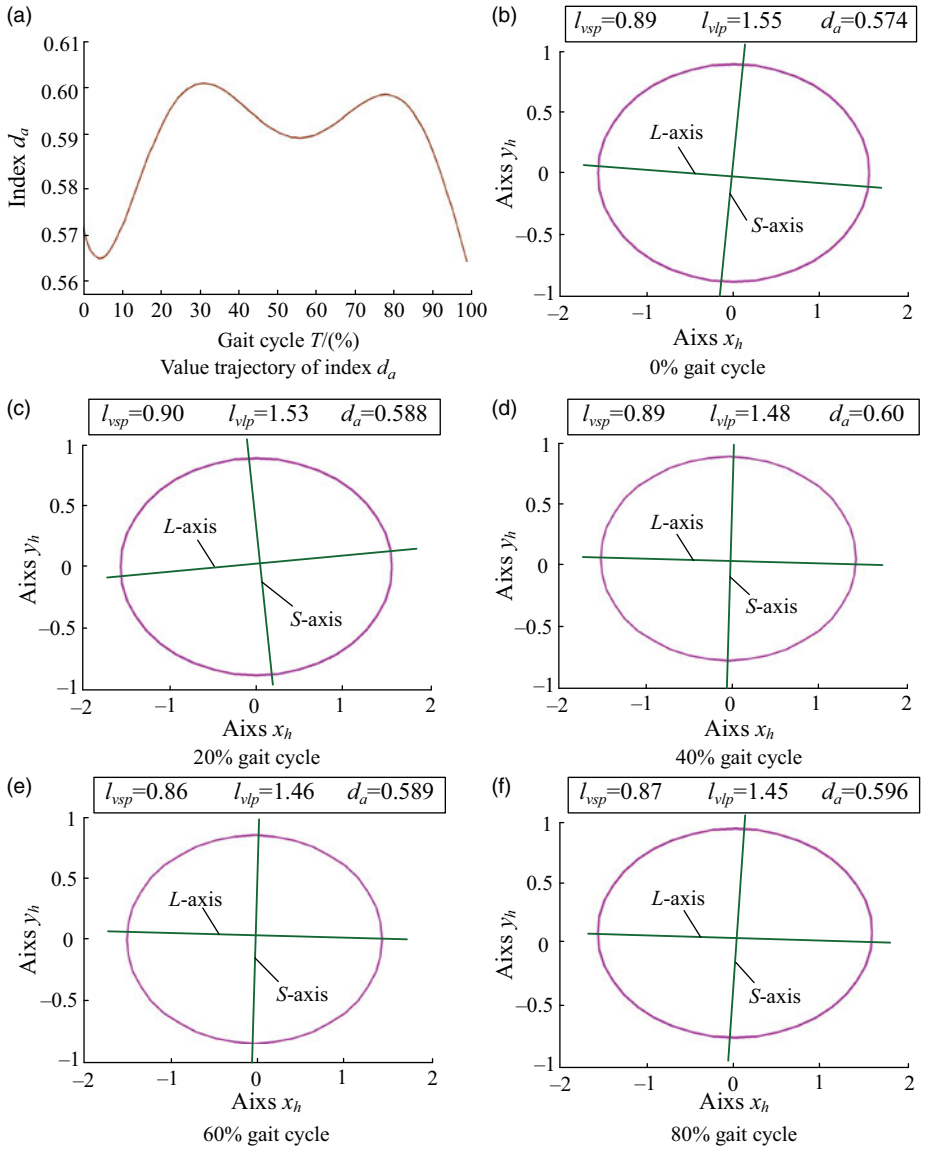

Fig. 6. Velocity ellipses and motion assistive isotropy d_a at 0%, 20%, 40%, 60% and 80% gait cycle T.

https://doi.org/10.1017/S0263574719001802 Published online by Cambridge University Press

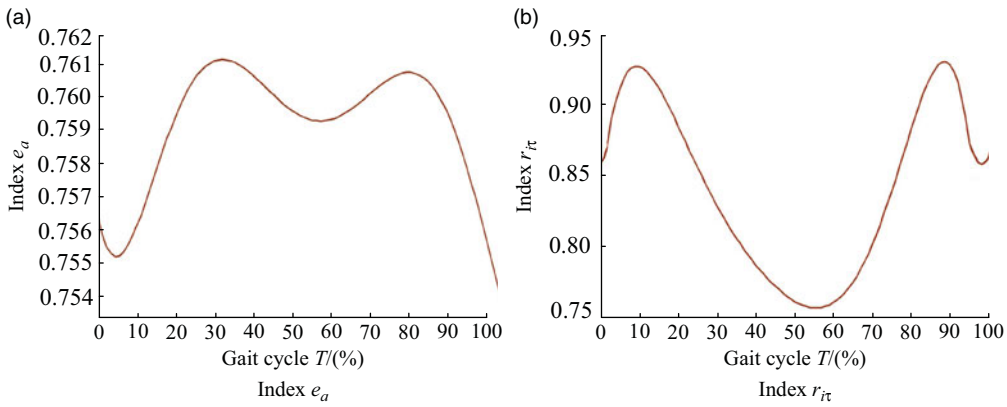

Fig. 7. Force transfer ratio e_a and isotropic force radius $r_{i\tau}$.

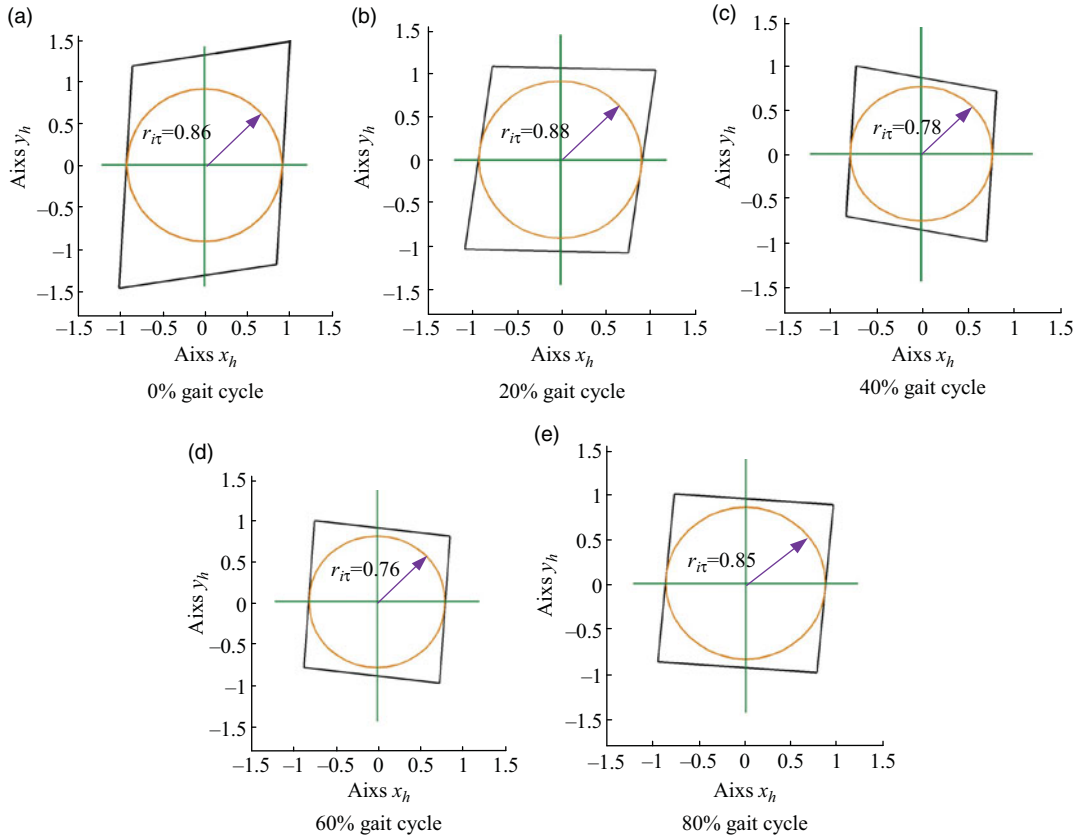

Fig. 8. Task-space force sets T_t and isotropic force radius $r_{i\tau}$ at 0%, 20%, 40%, 60% and 80% gait cycle T.

From Fig. 5, it can be seen that during a human gait cycle, the kinematic parameters of active and passive joints in the assistive mechanism change in their rated ranges (i.e., the absolute value of each joint angle is $< 30°$), and all the curves of those parameters have no mutation and sharp point. Fig. 6 shows that the minimal value of motion assistive isotropy d_a is equal to 0.562, and the range of index d_a corresponds to $d_a \in (0.5620.605)$, which indicates that the assistive mechanism is kinematically isotropic enough for hip motion assistance. As shown in Fig. 7a, the minimal value of force transfer ratio e_a equals 0.755, which indicates that the assistive mechanism has a high force transfer ratio. In addition, from the curve of index $r_{i\tau}$ shown in Fig. 7b, as well as the task-space force sets $\boldsymbol{T}_\tau$ and their inscribed circles shown in Fig. 8, it is known that the minimal value of $r_{i\tau}$ equals 0.770 and the assistive mechanism achieves high force assistive efficacy during hip AD/AB and FL/EX assistance.

https://doi.org/10.1017/S0263574719001802 Published online by Cambridge University Press

Compared with similar assistive mechanisms,[16–18,30] the proposed mechanism processes a novel parallel configuration, fine velocity and force assistive capability, and suitable for hip FL/EX and AD/AB motion assistance according to the obtained results. However, it should be highlighted that the components of parallel assistive mechanism are supposed to be rigid bodies, the flexible distortions of human muscles are assumed to be negligible, and the human body parameters as well as hip FL/EX and AD/AB motion patterns were obtained from a single healthy subject rather than elderly people. If these factors were to be taken into account, some issues would arise, affecting the obtained results. For instance, physical connections between the assistive mechanism and human body would not be rigid, the number of DOFs in the human–machine closed chain may be > 2, and the obtained gait patterns may not be representative of use cases. With these considerations, future work would focus on the detection of body parameters and typical gait patterns of elderly people, parameter optimization and structure design of the parallel assistive mechanism, particularly suitable human–machine connective parts to reduce flexible distortions of human muscles.

5. Conclusions

A parallel assistive mechanism with 2 active DOFs is proposed for assisting FL/EX and AD/AB movements of the human hip complex. Relevant velocity and force transfer matrices are established based on kinematic constraint equations of the human–machine system and three performance indices are introduced to evaluate velocity and transfer performance. During a typical gait assistive cycle, changing curves of the three indices are obtained by solving the kinematic models and the velocity/force mapping relationship. The results show that the parallel assistive mechanism has advantages of fine motion assistive isotropy, high force transfer ratio and large force isotropic radius, which indicates that the assistive mechanism is suitable for hip FL/EX and AD/AB assistance. The obtained results could be used as the primal reference for future research on parameter optimization and development of the parallel hip assistive mechanism.

Acknowledgements

This research is partially supported by the projects of National Natural Science Foundation of China (Nos. 51675008, 51705007), Natural Science Foundation of Beijing Municipality (Nos. 3171001, 17L20019) and Natural Science Foundation of Beijing Education Committee (No. KM201810005015).

References

1. J. Verghese, A. LeValley, C. B. Hall, M. J. Katz, A. F. Ambrose and R. B. Lipton, "Epidemiology of gait disorders in community-residing older adults," *J. Am. Geriatr. Soc.* **54**(2), 255–261 (2006).
2. R. S. Wilson, J. A. Schneider, L. A. Beckett, D. A. Evans and D. A. Bennett, "Progression of gait disorder and rigidity and risk of death in older persons," *Neurology* **58**(12), 1815–1819 (2002).
3. A. S. Reece and G. K. Hulse, "Duration of opiate exposure as a determinant of arterial stiffness and vascular age in male opiate dependence: a longitudinal study," *J. Clin. Pharm. Therap.* **39**(2), 158–167 (2014).
4. D. P. Ferris and C. L. Lewis, "Robotic Lower Limb Exoskeletons using Proportional Myoelectric Control," *Proceedings of the 31st Annual International Conference of the IEEE EMBS*, Minneapolis, Minnesota (2009) pp. 2119–2124.
5. C. L. Lewis and D. P. Ferris, "Invariant hip moment pattern while walking with a robotic hip exoskeleton," *J. Biomech.* **44**(5), 789–793 (2011).
6. F. Giovacchini, F. Vannetti, M. Fantozzi, M. Cempini, M. Cortese, A. Parri, T. Yan, D. Lefeber, and N. Vitielloa, "A light-weight active orthosis for hip movement assistance," *Robot. Auton. Syst.* **73**(2015), 123–134 (2015).
7. F. Giovacchini, M. Fantozzi, and M. Peroni, "A Light-Weight Exoskeleton for Hip Flexion-Extension Assistance," *Proceedings of the International Congress on Neurotechnology, Electronics and Informatics*, Algarve, Portugal (2013) pp. 194–198.
8. J. E. Pratt, B. T. Krupp, C. J. Morse, and S. H. Collins, "The Roboknee: An Exoskeleton for Enhancing Strength and Endurance during Walking," *Proceedings of the 2004 IEEE International Conference on Robotics & Automation*, New Orleans, LA, USA (2004) pp. 2430–2435.
9. A. Schiele Helm and D. F. C. T. Van, "Kinematic design to improve ergonomics in human machine interaction," *IEEE Trans. Neural Syst. Rehabilit. Eng.* **14**(4), 456–469 (2006).
10. N. Jarrasseì and G. Morel, "Connecting a human limb to an exoskeleton," *IEEE Trans. Robot.* **28**(3), 697–709 (2013).
11. M. J. Matariæ, J. Eriksson, D. J. Feil-Seifer and C. J. Winstein, "Socially assistive robotics for post-stroke rehabilitation," *J. Neuro Eng. Rehabil.* **4**(1), 1–9 (2007).

12. Q. Wu, X. Wang, F. Du and X. Zhang, "Design and control of a powered hip exoskeleton for walking assistance," *Int. J. Adv. Robot. Syst.* **12**(5), 1–12 (2015).
13. J. Olivier, A. Ortlieb, M. Bouri and H. Bleuler, "Mechanisms for actuated assistive hip orthoses," *Robot. Auton. Syst.* **73**(2015), 59–67 (2015).
14. J. Li, Z. Zhang, C. Tao, and R. Ji, "Structure design of lower limb exoskeletons for gait training," *Chinese J. Mech. Eng.* **28**(5), 878–887 (2015).
15. B. Fang, F. Sun, H. Liu, C. Tan and D. Guo, "A glove-based system for object recognition via visual-tactile fusion," *Sci. China Inf. Sci.* **62**(5), 674–685 (2019).
16. Z. Chi, M. Pan and D. Zhang, "Design of a Three DOFs MEMS-based Precision Manipulator," *Proceedings of the International Conference on Robot Vision and Signal Processing*, Kaohsiung City, Taiwan (2011) pp. 14–17.
17. Y. Yu, H. Tao, and W. Liang, "A Parallel Mechanism Used on Human Hip Joint Power Assist" *Proceedings of 2009 IEEE International Conference on Robotics and Biomimetics*, Guilin, China (2009) pp. 1007–1012.
18. Y. Yu and W. Liang, "Manipulability inclusive principle for hip joint assistive mechanism design optimization," *Int. J. Adv. Manuf. Technol.* **70**(5), 929–945 (2014).
19. J. Li, S. Li, L. Zhang, C. Tao and R. Ji, "Position solution and kinematic interference analysis of a novel parallel hip assistive mechanism," *Mech. Mach. Theory* **120**(2), 265–287 (2018).
20. T. Yoshikawa, "Manipulability of robotic mechanisms," *Int. J. Robot. Res.* **4**(2), 3–9 (1985).
21. L. Zhang, J. Li, P. Su, Y. Song, M. Dong and Q. Cao, "Improvement of human-machine compatibility of upper-limb rehabilitation exoskeleton using passive joints," *Robot. Auton. Syst.* **112**(2019), 22–31 (2019).
22. J. P. Merlet, "Jacobian, manipulability, condition number, and accuracy of parallel robots," *J. Mech. Des.* **128**(1), 199–206 (2006).
23. S. L. Chiu, "Task compatibility of manipulator postures," *Int. J. Robot. Res.* **74**(5), 13–21 (1988).
24. H. S. Kim and Y. J. Choi, "Forward/inverse force transmission capability analyses of fully parallel manipulators," *IEEE Trans. Robot. Autom.* **17**(4), 526–531 (2001).
25. T. J. Graettinger and N. H. Krogh, "The acceleration radius: a global performance measure for robotic manipulators," *IEEE J. Robot. Autom.* **4**(1), 60–69 (1988).
26. C. Y. Kim and Y. S. Yoon, "Task space dynamic analysis for multi-arm robot using isotropic velocity and acceleration radii," *Robotica* **15**(3), 319–329 (1997).
27. P. Chiacchio, S. Chiaverini, L. Sciavicco and B. Siciliano, "Task space dynamic analysis of multi-arm system configurations," *Int. J. Robot. Res.* **10**(6), 708–715 (1991).
28. Y. Kim and S. Desa, "Definition, determination, and characterization of acceleration sets for spatial manipulators," *Int. J. Robot. Res.* **12**(6), 572–587 (1993).
29. P. Chiacchio, Y. B. Vercelli and F. Pierrot, "Force polytope and force ellipsoid for redundant manipulators," *J. Robot. Syst.* **14**(8), 613–620 (1997).
30. W. Zhang, W. Zhang, D. Shi and X. Ding, "Design of hip joint assistant asymmetric parallel mechanism and optimization of singularity-free workspace," Mech. Mach. Theory **122**(2018), 389–403 (2018).